JGE (Jurnal Geofisika Eksplorasi)
Vol. 11 No. 02, July 2025 (135-150) https://doi.org/10.23960/jge.v11i2.493

LAST GLACIAL MAXIMUM – HOLOCENE RAINFALL SHIFTS IN THE WESTERN SAVU STRAIT BASED ON GEOCHEMICAL PROXIES

PERGESERAN CURAH HUJAN MAKSIMUM GLASIAL TERAKHIR – HOLOSEN DI SELAT SAVU BARAT BERDASARKAN PROKSI GEOKIMIA

Ryan Dwi Wahyu Ardi[1*], Aswan[2], Khoiril Anwar Maryunani[3], Eko Yulianto[4], Purna Sulastya Putra[5], Septriono Hari Nugroho[6], and Efrilia Mahdilah Nurhidayah[7]

[1,7]Geological Engineering Department, Faculty of Engineering, Universitas Jenderal Soedirman; Blater, Purbalingga, Central Java; (0281) 6586700;
[2,3]Geological Engineering Study Program, Institut Teknologi Bandung; Coblong, Bandung, West Java; (022) 250 2197;
[4,5,6]Research Center for Geological Disaster, National Research and Innovation Agency; Coblong, Bandung, West Java; +62811-1933-3639;

Received: 2025, June 13th
Accepted: 2025, July 15th

Keywords:
Australian–Indonesian Monsoon;
Glacial–interglacial climate change;
Indo-Pacific Warm Pool;
Rainfall reconstruction;
XRF elemental ratios.

Corespondent Email:
ryan.ardi@unsoed.ac.id

How to cite this article:
Ardi, R.D.W., Aswan, Maryunani, K.A., Yulianto, E., Putra, P.S., Nugroho, S.H., & Nurhidayah, E.M. (2025). Last Glacial Maximum – Holocene

Abstract. The Indo-Pacific Warm Pool significantly influences global atmospheric circulation, with tropical rainfall patterns highly sensitive to glacial–interglacial climate changes. During the Last Glacial Maximum (LGM), approximately 26,500 years before present, lower insolation, expanded ice sheets, and reduced sea levels weakened the Australian–Indonesian Monsoon (AIM) due to a southward shift of the Intertropical Convergence Zone (ITCZ). In contrast, the Holocene period experienced intensified monsoon systems and increased precipitation. However, high-resolution hydroclimate reconstructions from the western Savu Strait remain scarce. This study reconstructs rainfall variability from the LGM to the Holocene using geochemical proxies from sediment core ST10 (at 1 cm interval), located in the western Savu Strait. Three elemental ratios (Ti/Ca, K/Ca, and Rb/Sr) from X-ray fluorescence (XRF) core scanning were used to indicate terrigenous input, chemical weathering, and fluvial discharge. The age model was established using radiocarbon dating and stable isotope alignment with the Greenland ice core $\delta^{18}O$ record. Log-transformed elemental ratios reveal four intervals of increased rainfall: the LGM, Heinrich Event 1 (HE1), Younger Dryas to Early Holocene, and the Late Holocene. These periods are characterized by elevated Ti/Ca, K/Ca, and Rb/Sr values, suggesting enhanced monsoonal rainfall and continental runoff. Conversely, lower proxy values during the Early Deglaciation, Bølling–Allerød, and Mid-Holocene indicate drier climatic conditions. These patterns align with regional proxy records from southwest Sumba and the Timor Sea, confirming the reliability of elemental ratios

Rainfall Shifts in The Western Savu Strait Based On Geochemical Proxies. *JGE* (*Jurnal Geofisika Eksplorasi)*, 11(02), 135-150.

in reconstructing past hydroclimate variability. This study provides the first continuous record of rainfall shifts in the western Savu Strait from the LGM to Holocene and contributes to understanding long-term monsoon dynamics in southeastern Indonesia, highlighting the complex response of tropical hydroclimate to global climate forcing.

Abstrak. *Kolam Hangat Indo-Pasifik secara signifikan memengaruhi sirkulasi atmosfer global, dengan pola curah hujan tropis yang sangat sensitif terhadap perubahan iklim glasial-interglasial. Selama Maksimum Glasial Terakhir (LGM), sekitar 26.500 tahun sebelum sekarang, insolasi yang lebih rendah, lapisan es yang meluas, dan permukaan laut yang berkurang melemahkan Monsun Australia-Indonesia (AIM) karena pergeseran ke selatan dari Zona Konvergensi Intertropis (ITCZ). Sebaliknya, periode Holosen mengalami sistem monsun yang intensif dan peningkatan curah hujan. Namun, rekonstruksi hidroklimat resolusi tinggi dari Selat Sawu bagian barat masih langka. Studi ini merekonstruksi variabilitas curah hujan dari LGM hingga Holosen menggunakan proksi geokimia dari inti sedimen ST10 (pada interval 1 cm), yang terletak di Selat Sawu bagian barat. Tiga rasio unsur (Ti/Ca, K/Ca, dan Rb/Sr) dari pemindaian inti fluoresensi sinar-X (XRF) digunakan untuk menunjukkan masukan terigen, pelapukan kimia, dan debit fluvial. Model usia ditetapkan menggunakan penanggalan radiokarbon dan penyelarasan isotop stabil dengan catatan $\delta^{18}O$ inti es Greenland. Rasio unsur yang ditransformasikan secara logaritma menunjukkan empat interval peningkatan curah hujan: LGM, Peristiwa Heinrich 1 (HE1), Dryas Muda hingga Holosen Awal, dan Holosen Akhir. Periode-periode ini dicirikan oleh nilai Ti/Ca, K/Ca, dan Rb/Sr yang lebih tinggi, yang menunjukkan peningkatan curah hujan monsun dan limpasan benua. Sebaliknya, nilai proksi yang lebih rendah selama Deglasiasi Awal, Bølling–Allerød, dan Holosen Tengah menunjukkan kondisi iklim yang lebih kering. Pola-pola ini selaras dengan catatan proksi regional dari Sumba barat daya dan Laut Timor, yang menegaskan keandalan rasio unsur dalam merekonstruksi variabilitas hidroklimat masa lalu. Studi ini memberikan catatan berkelanjutan pertama mengenai pergeseran curah hujan di Selat Savu bagian barat dari LGM hingga Holosen dan berkontribusi terhadap pemahaman dinamika monsun jangka panjang di Indonesia bagian tenggara, yang menyoroti respons kompleks hidro-iklim tropis terhadap pemaksaan iklim global.*

1. INTRODUCTION

The Indo-Pacific warm pool plays a central role in shaping global atmospheric circulation, and its rainfall patterns are particularly responsive to glacial–interglacial climate variability (Yu et al., 2023; Cui et al., 2025). Evidence from the Last Glacial Maximum (LGM; ~26,500 years Before Present/BP) indicates that reduced insolation, expanded ice sheets, and lower sea levels shifted the Intertropical Convergence Zone (ITCZ) southward, leading to weaker monsoonal activity and a decline in the strength of the Australian–Indonesian Monsoon (AIM) (Di Nezio et al., 2016; Scroxton et al., 2022). With the onset of the Holocene, these conditions reversed: rainfall increased, monsoonal circulation strengthened, and large-scale adjustments occurred in ocean–atmosphere interactions (Ardi et al., 2020; Hendrizan et al., 2023; Lowry & McGowan, 2024).

While research on tropical hydroclimate evolution has expanded in recent decades, detailed paleoenvironmental records from the western Savu Strait are still scarce. Insights from nearby regions, such as southwest Sumba (Ardi et al., 2020) and

Flores (Griffiths et al., 2009; Ayliffe et al., 2013), point to substantial shifts in rainfall through the Last Deglaciation and into the Holocene. These studies generally suggest drier conditions during the LGM, followed by a rise in precipitation during the early Holocene. Even so, rainfall distribution across the maritime continent is far from uniform, emphasizing the value of site-specific reconstructions for improving our understanding of Australian–Indonesian Monsoon dynamics.

Geochemical records from marine sediments provide valuable insights into past environmental and hydrological changes, particularly when analyzed using high-resolution X-ray fluorescence (XRF) scanning. In tropical regions, elemental ratios such as titanium to calcium (Ti/Ca), potassium to calcium (K/Ca), and rubidium to strontium (Rb/Sr) are commonly applied to reconstruct variations in terrestrial input, weathering intensity, and river discharge (Yu et al., 2023; Ardi et al., 2020). While titanium and potassium largely reflect detrital input from river systems, calcium and strontium are more indicative of carbonate production within the marine environment. Periods of increased Ti/Ca and K/Ca are typically interpreted as reflecting stronger rainfall and runoff, while higher Rb/Sr ratios tend to indicate intensified chemical weathering, often associated with wetter climatic conditions.

This study explores hydroclimate variability from the LGM through the Holocene in the western Savu Strait (**Figure 1**). Our reconstruction relies on elemental ratios (Ti/Ca, K/Ca, and Rb/Sr) obtained from XRF core scanning, which serve as proxies for changes in rainfall and terrestrial input. By tracing the temporal evolution of these signals, we aim to capture shifts in precipitation intensity and riverine discharge associated with glacial–interglacial climate transitions. In doing so, the study provides fresh insight into the long-term behavior of the Indonesian monsoon system and helps close a notable spatial gap in paleo-rainfall records from the eastern Indian Ocean.

2. LITERATURE REVIEW

The Indo-Pacific region, encompassing the Lesser Sunda Islands and Wallacea, is shaped by complex ocean–atmosphere interactions influenced by the by monsoon systems (AIM), seasonal shifts of the ITCZ, and major surface currents. During the LGM, global sea level was about 120 m lower, exposing large portions of the Sunda Shelf and narrowing critical passages such as the Makassar Strait. These changes substantially weakened the Indonesian Throughflow (ITF), leading to cooler sea surface temperatures, higher salinity, and reduced freshwater input in the region (Hendrizan et al., 2017; Xu et al., 2010). Last Deglaciation and Early Holocene records show abrupt hydrological intensification, driven by rising sea levels and ITF re-establishment (Mohtadi et al., 2011; Sprintall & Révelard, 2014; Hendrizan et al., 2017; Feng et al., 2018). Concurrent shifts in the Intertropical Convergence Zone (ITCZ) during the Early Holocene brought increased monsoonal rainfall and river discharge across Indonesia (Hendrizan et al., 2017).

In modern climate conditions, seasonal monsoon cycles drive significant variability in regional hydroclimate and ocean currents of the Indonesian region (**Figure 1**). During austral winter (June–August), the southeast monsoon sends dry air from Australia, generating westward currents including the South Java Current (SJC) and Karimata Strait Throughflow (KSTF), while reinforcing the Makassar Strait Throughflow (Sprintall et al., 2009; Xu et al., 2010) (**Figure 1**). Additionally, the Leeuwin Current, carrying warm, low-salinity water south along Western Australia, peaks in strength under these conditions (Feng et al., 2003). During Austral summer (December–February), northwesterly monsoon winds reverse this circulation: the SJC weakens or reverses, the ITCZ shifts southward, and rainfall increases across southern Indonesia (**Figure 1**).

3. RESEARCH METHODS

Sediment core ST10 (gravity core) was collected from the western Savu Strait during the 2016 Widya Nusantara Expedition (E-WIN) aboard the Baruna Jaya

VIII research vessel (**Table 1**). The expedition was conducted by the Research Center for Oceanography, Indonesian Institute of Sciences (LIPI), which is now part of the Research Center for Geological Disaster, National Research and Innovation Agency (BRIN). The core was analyzed at 1 cm intervals using a Thermo NITON XL3t 500 Field Portable X ray Fluorescence (FP XRF) spectrometer, yielding 136 data points. This study focuses on the upper interval of the core, spanning approximately 26.5 ka BP to the present, covering the LGM to the Holocene period.

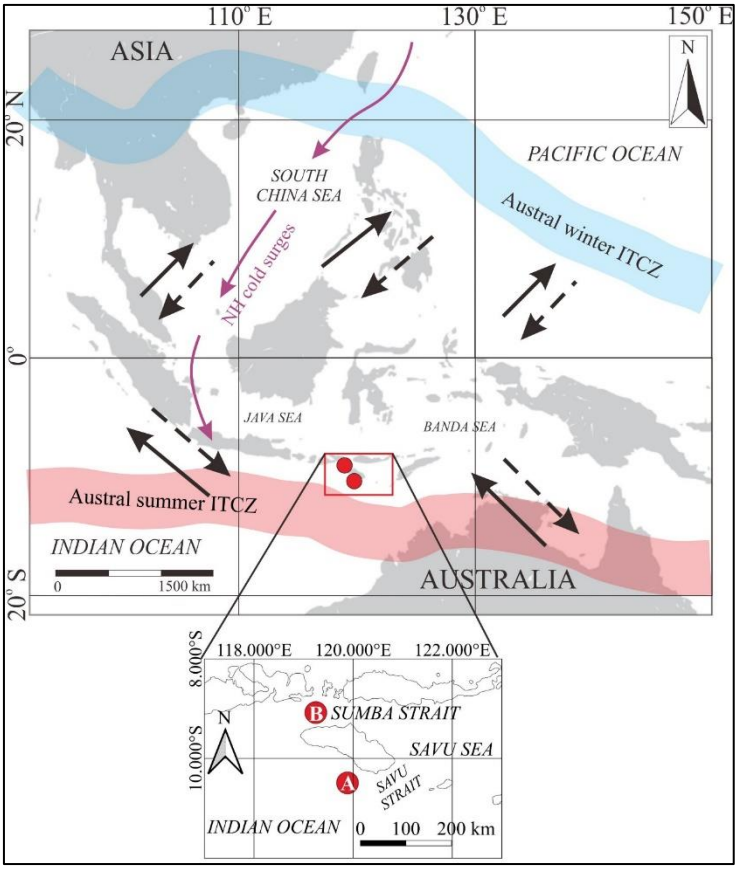

Figure 1. The figure illustrates the regional climate and oceanographic setting of Indonesia (adapted from Gordon, 2005; Qu et al., 2005; Sprintall et al., 2009; Kuhnt et al., 2015; Di Nezio et al., 2016; Wang et al., 2017; Bayhaqi et al., 2019). The red rectangle outlines the study area, with core ST10 (this study, A) and core ST08 (Ardi et al., 2020, B) shown by white circles. Blue arrows indicate ITF pathways originating from the North Pacific, while purple arrows represent inflows from the South Pacific. Cyan arrows mark seasonally reversing currents, including the SJC, KSTF, and LC. Dashed lines show the Australian-Indonesian Summer Monsoon (AISM), and solid lines indicate the Australian-Indonesian Winter Monsoon (AIWM). The ITCZ is shown by red shading in Austral summer and light blue shading in austral winter, while yellow shading highlights the Sunda and Sahul shelves.

Table 1. Sediment core used in this study.

Core	Location	Coordinate		Depth (m)
		Latitude (^{0}E)	Longitude (^{0}S)	
ST10	Western Savu Strait	119.885	10.491	1004

3.1. Geochemical Proxies (Elemental Ratios)

To reconstruct past changes in rainfall and sediment dynamics in the Australian–Indonesian monsoon (AIM) region, this study utilizes log-transformed elemental ratios derived from semi-quantitative FP-XRF measurements. The use of elemental ratios minimizes matrix effects and enhances data comparability, while logarithmic transformation addresses skewness in ratio distributions (e.g. Tjallingii et al., 2007; Gebregiorgis et al., 2020). This research focuses on three elemental ratios: Ti/Ca and K/Ca, which reflect terrigenous input carried by rivers, and Rb/Sr, which serves as an indicator of physical weathering and variations in sediment grain size.

Higher Ti/Ca and K/Ca ratios are interpreted as reflecting stronger riverine input driven by intensified monsoonal rainfall, a pattern consistent with previous paleomonsoon reconstructions (Kuhnt et al., 2015; Setiawan et al., 2015; Gebregiorgis et al., 2020). Titanium (Ti) mainly originates from the weathering of mafic and ultramafic rocks, while potassium (K) is typically sourced from mica-bearing lithologies (Nesbitt et al., 1980). Calcium (Ca), derived predominantly from marine biogenic carbonates, is used as a denominator to normalize detrital input and reduce the effect of carbonate dilution (Gebregiorgis et al., 2020).

The Rb/Sr ratio provides an additional measure of physical weathering. Rubidium (Rb) tends to be enriched in clay-sized particles, while strontium (Sr) is more closely associated with coarser carbonate phases. Elevated Rb/Sr values therefore indicate enhanced mechanical erosion and increased delivery of fine-grained terrigenous material (Chen et al., 1999; Miriyala et al., 2017). Because carbonate formations are present on Sumba Island, the marine origin of Ca was further confirmed by low correlation coefficients (R^2) between Ca and both Ti and K in linear regressions, supporting its interpretation as a biogenic marine denominator (Gebregiorgis et al., 2020) (**Figure 2**).

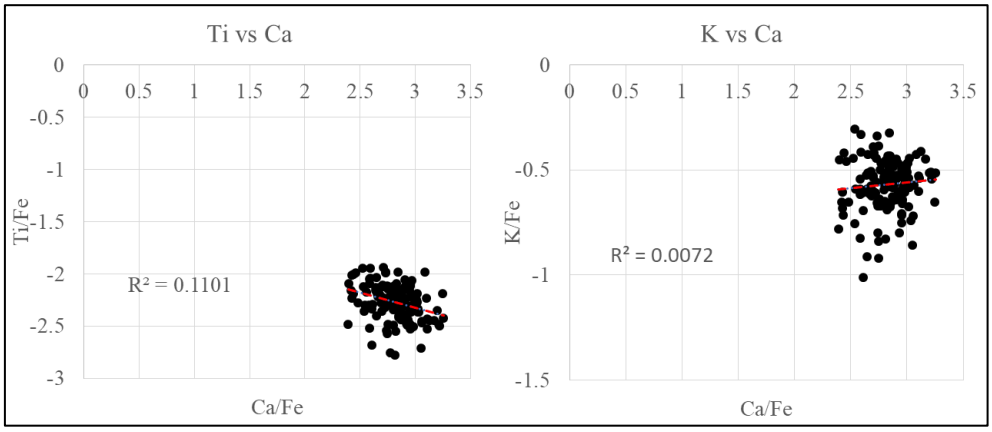

Figure 2. Linear correlations between Ti and Ca, as well as K and Ca, after normalizing all elements to Fe, show low correlation coefficients. This supports the interpretation that Ca is mainly derived from marine biogenic sources, while Ti and K represent terrigenous contributions.

3.2. Age Model

The age model for sediment core ST10 was constructed using a Bayesian age–depth approach, with reference points constrained by absolute age controls. These include Accelerator Mass Spectrometry (AMS) radiocarbon dates measured on the planktonic foraminifera Neogloboquadrina dutertrei, along with a stratigraphic tie-point established by aligning the $\delta^{18}O$ record of Globigerinoides ruber with the 20-year averaged $\delta^{18}O$ profile from the North Greenland Ice Core Project (NGRIP), based on the Greenland Ice Core Chronology 2005 (GICC05) (Andersen et al., 2007).

4. RESULTS AND DISCUSSION

Megascopic observations show that the ST10 sediment core is dominated by silt from the surface down to 96 cm, underlain by a thicker sand-rich unit between 96 and 137 cm. The uppermost section (0–28 cm) is characterized by gray silt with abundant foraminifera and mollusk remains. Below this, the 28–58 cm interval is also composed of silt, but with noticeably fewer foraminifera and mollusks than in the overlying layer. Between 58 and 96 cm, the silt is intercalated with very fine sand, gray in color, and contains foraminifera and mollusks. The 96–137 cm interval is composed of dark gray, very fine sand dominated by foraminiferal tests (90%), with minor components of heavy minerals such as dark mica and magnetite (7.5%), and mollusk fragments (2.5%) (**Figure 3**).

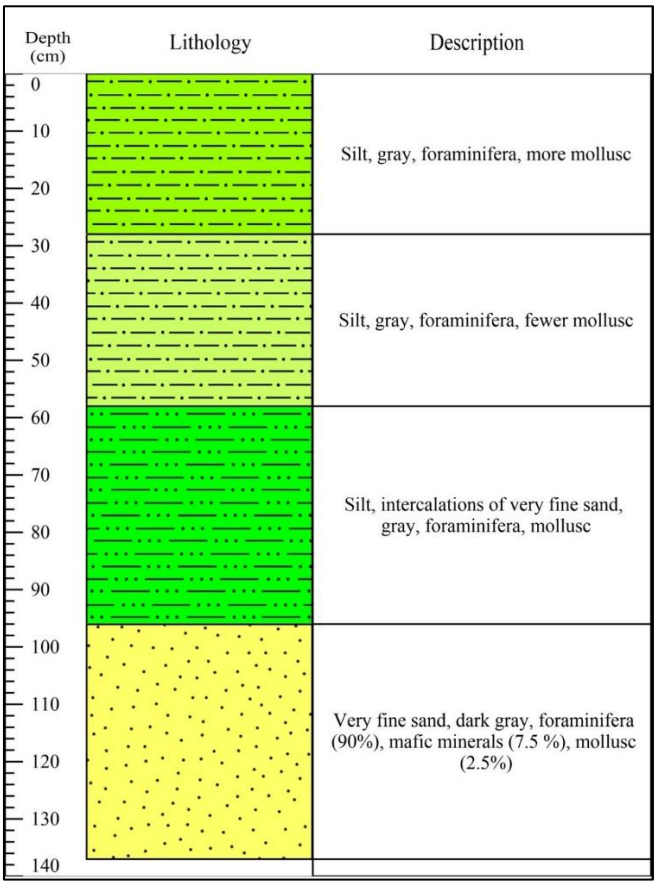

Figure 3. Stratigraphy of sediment core ST10 based on megascopic observation, showing silt-dominated sediments from 0–96 cm with intercalated very fine sand at 58–96 cm interval, and a thick interval of very fine sand from 96–137 cm.

4.1. Age Model Result

Absolute age data used for age-depth modelling are presented in **Table 2**. For core ST10, a tie-point was derived from the alignment of $\delta^{18}O$ values in Globigerinoides ruber with the 20-year averaged $\delta^{18}O$ record from the NGRIP ice core, based on the GICC05 timescale (Andersen et al., 2007). This tie point corresponds to the Pleistocene–Holocene boundary at 11.65 ka BP, which also marks the transition between Marine Isotope Stage (MIS) 2 and MIS 1 (Shackleton, 1987) (**Figure 4**).

The age-depth model was constructed using a Bayesian framework implemented through the 'rbacon' package (version 2.4.2) in R (R Core Team, 2013; Blaauw & Christen, 2011; Blaauw, 2010) (**Figure 5**). This approach allows for probabilistic modeling of sediment accumulation rates and provides a robust chronology for interpreting paleoenvironmental changes from the LGM to the Holocene.

Table 2. Absolute age data of core ST10.

Lab	Methods	Depth	Material	14C age (BP)	Calibrated 14C age BP
Brown	$\delta^{18}O$ GICC05	31.5 cm	Foraminifera: *Globigerinoides ruber*	11650 ± 99	–
Nosams	AMS ^{14}C	40–41 cm	Foraminifera: *Neogloboquadrina dutertrei*	13850 ± 55	16583–15525
Beta	AMS ^{14}C	136–137 cm	Foraminifera: *Neogloboquadrina dutertrei*	33280 ± 200	35721–34286

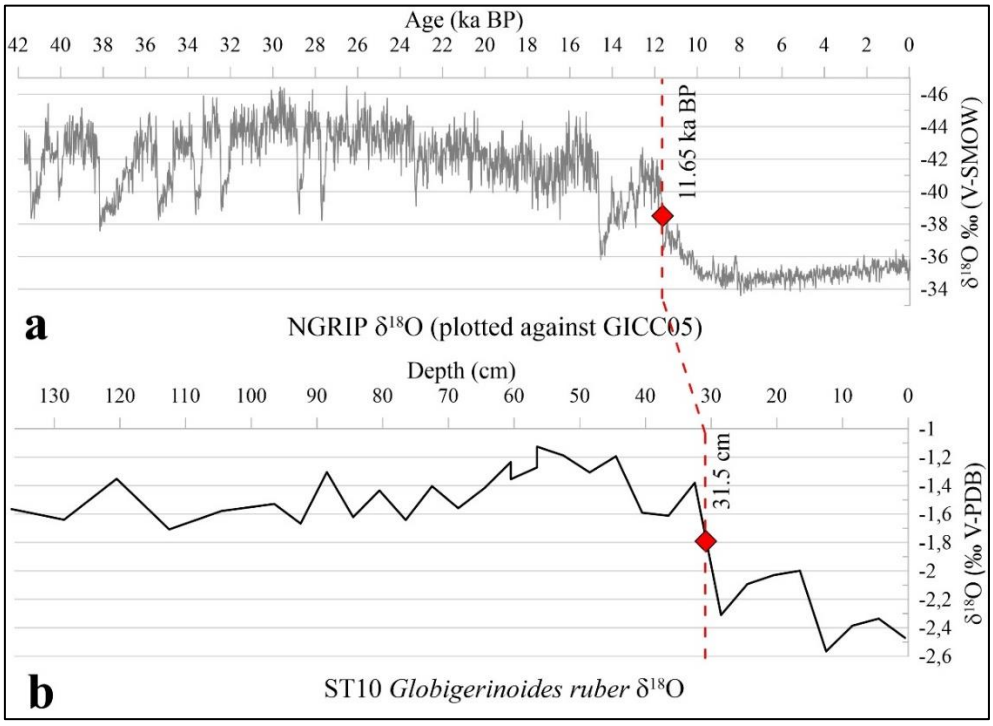

Figure 4. Correlation between the NGRIP GICC05 $\delta^{18}O$ record (reference year: 1950 AD) from Andersen et al. (2007) (a) and the *Globigerinoides ruber* $\delta^{18}O$ record from core ST10 (b). Red diamonds mark the tie points used for correlation (Pleistocene–Holocene boundary).

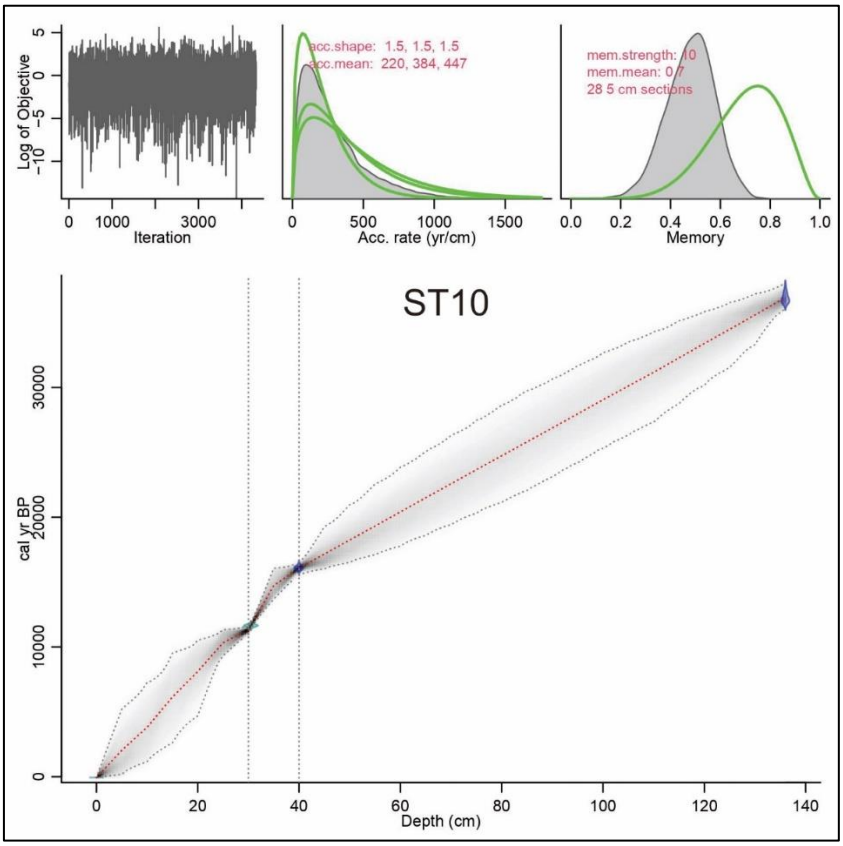

Figure 5. The Bayesian age–depth model for core ST10 was generated using the *rbacon* package (version 2.4.2) in R (Blaauw, 2010; R Core Team, 2013), following the framework of Blaauw and Christen (2011). In the upper panels, the left plot shows the Markov chain Monte Carlo (MCMC) iterations, while the middle and right plots display the prior distributions (green curves) alongside the posterior outcomes (grey histograms) for accumulation rate and memory, respectively (Blaauw, 2010). The lower panel illustrates the calibrated radiocarbon ages (transparent blue) and the modeled age–depth relationship, where darker grey tones denote higher probability ranges, dashed grey lines mark the 95% confidence intervals, and the red curve indicates the mean-based 'best' fit model (Blaauw, 2010).

4.2. LGM–Holocene Rainfall Shifts based on Geochemical Proxies

This study focuses on three log-transformed elemental ratios which are Ti/Ca, K/Ca, and Rb/Sr, derived from semi-quantitative FP-XRF measurements. These ratios are interpreted as proxies for terrigenous input (Ti/Ca and K/Ca) and physical weathering (Rb/Sr). To investigate their relationship with broader climatic shifts, the variability of these geochemical proxies is compared with the $\delta^{18}O$ record from the NGRIP, based on the GICC05 timescale (Andersen et al., 2007). This comparison enables a detailed assessment of how regional sedimentary signals in the western Savu Strait relate to global climate events from the LGM through the Holocene (**Figure 6**).

The Ti/Ca and K/Ca ratios display coherent fluctuations throughout the core, with both ratios broadly tracking changes in terrigenous material delivery to the site. Elevated values in these ratios are interpreted as reflecting increased fluvial input from surrounding landmasses, primarily driven by enhanced AIM rainfall. Four distinct periods show relatively higher K/Ca and Ti/Ca values: (1) LGM (~26.5–22 ka BP) (ln Ti/Ca: ~-4.7; ln K/Ca: ~-3.15), (2)

Heinrich Event 1 (HE1) (~18–15 ka BP) (ln Ti/Ca: ~-4.9; ln K/Ca: ~-3.3), (3) the Younger Dryas (YD) to Early Holocene (EH) (~13–7 ka BP) (ln Ti/Ca: ~-4.9; ln K/Ca: ~-3.35), and (4) the Late Holocene (LH) -(after ~3 ka BP) (ln Ti/Ca: ~-4.8; ln K/Ca: ~-3.15) (**Figure 6**). These intervals likely represent times of intensified continental runoff and greater detrital supply, indicating wetter climatic conditions across the region. In contrast, three periods, namely the Early Deglaciation (~22–18 ka BP) (ln Ti/Ca: ~-5.15; ln K/Ca: ~-3.45), the Bølling–Allerød Interstadial (B-A) (~15–13 ka BP) (ln Ti/Ca: ~-5; ln K/Ca: ~-3.45), and the Mid-Holocene (MH) (~7–3 ka BP) (ln Ti/Ca: ~-5.15; ln K/Ca: ~-3.55), exhibit relatively lower Ti/Ca and K/Ca values, suggesting reduced terrigenous input and implying drier climatic conditions during these intervals (**Figure 6**).

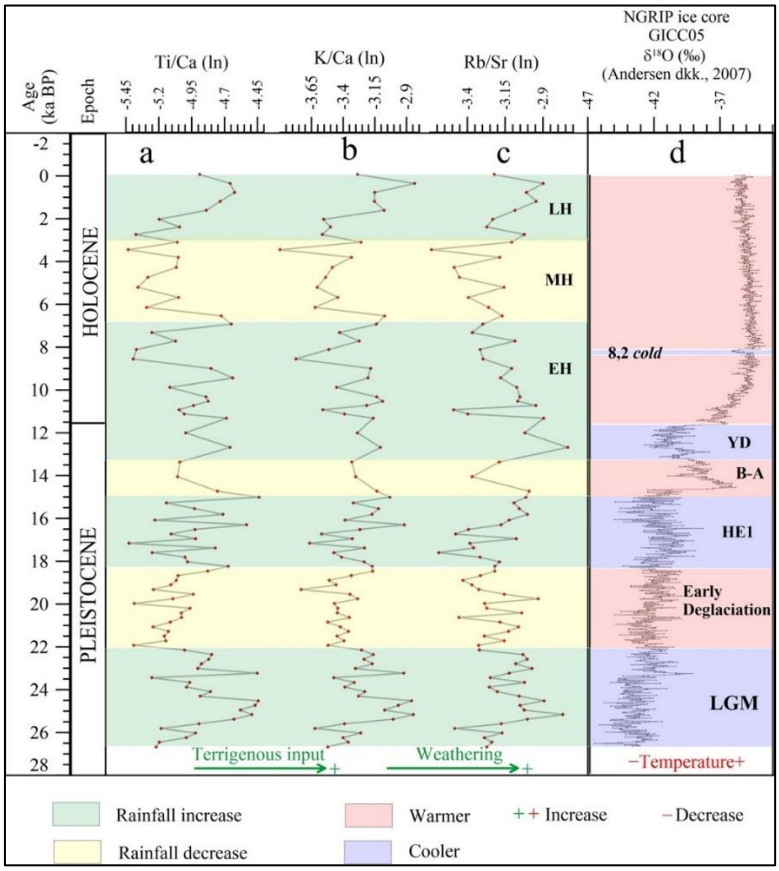

Figure 6. Geochemical proxy records from core ST10: Ti/Ca (a), K/Ca (b), and Rb/Sr (c), compared to the NGRIP $\delta^{18}O$ record plotted on the GICC05 age scale (Andersen et al., 2007). These elemental ratios serve as indicators of terrigenous input and physical weathering variability, while the NGRIP $\delta^{18}O$ record provides a reference for Northern Hemisphere climate changes.

The Rb/Sr ratio, used here as a proxy for physical or mechanical weathering, exhibits trends largely parallel to those of K/Ca and Ti/Ca. The Rb/Sr ratio, used here as a proxy for physical or mechanical weathering, exhibits trends largely parallel to those of K/Ca and Ti/Ca. Four periods show relatively higher Rb/Sr values: (1) LGM (~26.5–22 ka BP) (ln Rb/Sr: -3.1), (2) HE1 (~18–15 ka BP) (ln Rb/Sr: -3.05), (3) YD to EH (~13–7 ka BP) (ln Rb/Sr: -3.1), and (4) LH (after ~3 ka BP) (ln Rb/Sr: -3.1) (**Figure 6**). These intervals likely represent enhanced physical weathering and increased detrital input, consistent with wetter climatic conditions and intensified

runoff. Rubidium, being more concentrated in fine-grained clay minerals, and strontium, commonly associated with coarser carbonate or detrital phases, respond differently to erosion and sorting processes. Elevated Rb/Sr values correspond with periods of stronger mechanical weathering, consistent with increased precipitation and surface runoff during the aforementioned high-rainfall intervals (Chen et al., 2008). In contrast, three periods, namely the Early Deglaciation (22–18 ka BP) (ln Rb/Sr:-3.25), B-A (~15–13 ka BP) (ln Rb/Sr: -3.25), and MH (~7–3 ka BP) (ln Rb/Sr: -3.35), exhibit relatively lower Rb/Sr values, indicating reduced physical weathering and suggesting drier environmental conditions during these times. These results suggest that Rb/Sr is a reliable indicator of hydrodynamically enhanced sediment transport and erosion in this setting.

Taken together, the three geochemical proxies identify four periods of increased terrigenous input and weathering which include LGM (~26.5–22 ka BP), HE1 (~18–15 ka BP), YD to EH (~13–7 ka BP), and LH (after ~3 ka BP), interpreted as phases of higher rainfall and intensified AIM activity (**Figure 6**). In contrast, three intervals which are Early Deglaciation (~22–18 ka BP), B-A (~15–13 ka BP), and MH (~7–3 ka BP), are marked by lower K/Ca, Ti/Ca, and Rb/Sr values, indicating reduced terrigenous influx and physical weathering, which are interpreted as periods of weaker AIM rainfall (**Figure 6**).

4.3. Climatic Drivers of Monsoonal Rainfall Shifts in the Western Savu Strait: Insights from Multi-Proxy Correlations

The elemental ratio of ST10 (represented by K/Ca), K/Ca ratio of ST08 (off southwest Sumba) (Ardi et al., 2020), SO185-18460 (Timor Sea) (Kuhnt et al., 2015), $\delta^{18}O$ record from the NGRIP based on the GICC05 timescale (Andersen et al., 2007), EPICA Dronning Maud Land (EDML) $\delta^{18}O$ (‰ V-SMOW) (EPICA Community Members, 2006), Austral summer insolation at 20°S (W/m^2) (Berger, 1978), and relative sea level (Siddall et al., 2003; Arz et al., 2007) were also correlated to investigate the mechanisms responsible for rainfall shifts in the western Savu Strait (**Figure 7**).

The intensification of (AIM) rainfall during globally colder periods, specifically LGM (~26.5–22 ka BP), HE1 (~18–15 ka BP), and YD (~13.5–11.65 ka BP), has also been recorded at other locations in southern Indonesia, such as off southwest Sumba (ST08 core) (Ardi et al., 2020) and the Timor Sea (core SO185-18460) (Kuhnt et al., 2015) (**Figure 7**). These proxy records consistently show elevated K/Ca ratios during these glacial periods, indicating increased terrigenous input driven by intensified monsoonal rainfall. In contrast, periods of reduced AIM rainfall were also detected at these locations during the Early Deglaciation (22–18 ka BP) and B-A (~15–13 ka BP), as reflected by lower K/Ca ratios and decreased ln Rb/Sr values, indicating reduced terrigenous input and weaker monsoonal activity (Griffiths et al., 2009; Stott et al., 2007; Xu et al., 2010) (**Figure 7**).

Periods of unusually high rainfall during globally cooler conditions were likely associated with a southward migration of the ITCZ during the Austral summer. Both proxy records and climate model results indicate that, in these stadial intervals, the ITCZ moved toward northern Australia, placing southern Indonesia directly beneath its main convective belt and thereby intensifying monsoonal rainfall (Ayliffe et al., 2013; Mohtadi et al., 2017) (**Figure 8**). This displacement was largely driven by the expansion of Northern Hemisphere ice sheets, which strengthened interhemispheric temperature gradients and subsequently modified large-scale atmospheric circulation, including the Hadley cell (Broccoli et al., 2006; McGee et al., 2014).

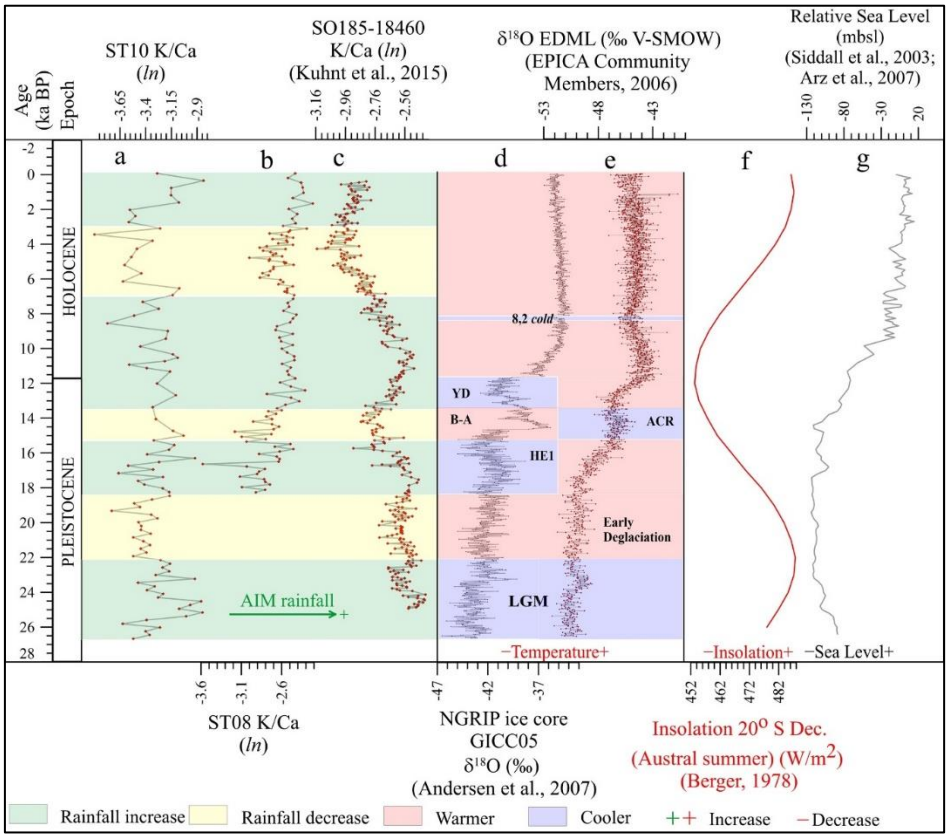

Figure 7. Comparison of the K/Ca ratio from core ST10 (a) with K/Ca records from core ST08 (off southwest Sumba) (Ardi et al., 2020) (b) and core SO185-18460 (Timor Sea) (Kuhnt et al., 2015) (c). Also shown are the NGRIP $\delta^{18}O$ record on the GICC05 timescale (Andersen et al., 2007) (d), EPICA Dronning Maud Land (EDML) $\delta^{18}O$ record (‰ V-SMOW) (EPICA Community Members, 2006) (e), Austral summer insolation at 20°S (W/m^2) (Berger, 1978) (f), and global relative sea level (Siddall et al., 2003; Arz et al., 2007) (g). These datasets are integrated to explore the climatic drivers and mechanisms influencing rainfall variability in the western Savu Strait.

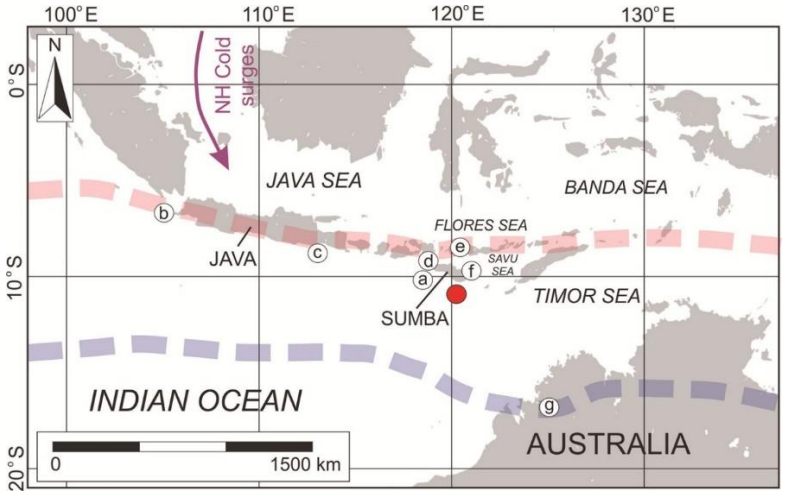

Figure 8. Schematic of the Austral summer ITCZ under varying hydroclimatic conditions. The red dashed line marks its extent during drier periods, the blue dashed line during wetter periods. Core ST10 is shown by the red circle (Ardi et al., 2020).

The southward displacement of the Austral summer ITCZ during glacial periods was further reinforced by intensified cold surges associated with a stronger East Asian winter monsoon. These northeasterly outbreaks advected cold, dry air from East Asia, enhancing low-level convergence and convective activity over the southern Maritime Continent (Suppiah & Wu, 1998; Lim et al., 2017). By strengthening cross-equatorial pressure gradients and facilitating southward moisture transport, cold surges pushed the ITCZ further south (Wang et al., 2005; Lim et al., 2017) (**Figure 8**). Intensified surges thus contributed to both increased rainfall over southern Indonesia and the persistence of a southward-shifted ITCZ during glacial intervals.

During interstadial or drier phases, including the Early Deglaciation and B-A, the Austral summer ITCZ shifted northward to the latitude of the Lesser Sunda Islands, placing the western Savu Strait outside its convective core (**Figure 8**). Reduced or absent cold surge activity further limited low-level convergence and southward moisture transport into the southern Maritime Continent. The combined effect of a northerly ITCZ and weakened cold surges resulted in reduced AIM rainfall over southern Indonesia. Hydroclimate records from southwest Sumba and the Timor Sea therefore indicate that AIM variability from the LGM to the Holocene was primarily governed by ITCZ latitude and cold surge activity.

The intensification of AIM rainfall during the Early Holocene was most likely linked to the rapid postglacial sea-level rise that fully submerged the Sunda and Sahul shelves, significantly expanding the regional sea surface area and enhancing evaporation rates (Hanebuth et al., 2000; Bird et al., 2005) (**Figure 7**). This widespread inundation increased atmospheric moisture availability, contributing to stronger monsoonal rainfall over southern Indonesia during the Early Holocene.

In contrast, the reduction in AIM rainfall during MH was likely associated with the delayed response to decreasing Austral summer insolation (**Figure 7**). As orbital precession gradually reduced solar radiation at southern tropical latitudes, evaporation and monsoonal convection weakened, resulting in drier climatic conditions (Linsley et al., 2010; Griffiths et al., 2009). The subsequent increase in AIM rainfall during LH corresponds with a gradual rise in Austral summer insolation, which enhanced surface heating and evaporation, thereby strengthening monsoonal precipitation (Partin et al., 2007; Ayliffe et al., 2013) (**Figure 7**).

However, the latitudinal migration of the Austral summer ITCZ throughout the Holocene remains uncertain. Unlike the pronounced ITCZ displacements during the Last Deglaciation, Holocene climatic variations were comparatively subdued, potentially limiting large-scale shifts in the ITCZ (McGee et al., 2014; Denniston et al., 2016). Further regional evidence is needed to clarify the role of ITCZ shifts in shaping monsoonal rainfall variability across the tropical Indo-Pacific during the Holocene.

These results demonstrate the strong sensitivity of sedimentation in the western Savu Strait to large-scale climate variability and underscore the utility of elemental ratios as robust proxies for reconstructing past hydroclimate in the tropical Indo-Pacific. Ratios such as Ti/Ca, K/Ca, and Rb/Sr primarily reflect changes in terrigenous input, which are closely tied to variations in monsoonal rainfall and continental runoff (Holbourn et al., 2005; Kuhnt et al., 2015). Intensified AIM rainfall promotes enhanced weathering and erosion on surrounding landmasses, increasing the flux of lithogenic material to the ocean and producing higher detrital element ratios in marine sediments (Mohtadi et al., 2017).

In the Indonesian seas, where direct hydrological records are limited, sedimentary geochemical proxies provide crucial archives for reconstructing past variations in rainfall, river discharge, and atmospheric circulation. When integrated with complementary indicators such as stable isotopes and foraminiferal assemblages, these proxies allow for more robust reconstructions of paleomonsoon

dynamics and ITCZ shifts (Griffiths et al., 2009; Linsley et al., 2010). Given the central role of the tropical Indo-Pacific in regulating global ocean–atmosphere interactions, including ENSO and the IOD, high-resolution paleoenvironmental records from this region are especially valuable (Partin et al., 2007; Mohtadi et al., 2017).

5. CONCLUSION

This study uses semi-quantitative FP-XRF measurements of Ti/Ca, K/Ca, and Rb/Sr ratios from marine sediment cores to reconstruct past rainfall variability in the western Savu Strait. These elemental ratios serve as proxies for terrigenous input and physical weathering, reflecting changes in continental runoff and monsoonal strength. The results identify four wetter phases (LGM, HE1, YD–EH, and LH), linked to southward ITCZ displacement, intensified cold surges, sea-level rise, and orbital insolation forcing. Drier intervals during Early Deglaciation, B-A, and MH reflect weakened monsoon activity. This approach offers an efficient means of tracking hydroclimate shifts, though reliance on semi-quantitative XRF data limits geochemical precision. Future studies should integrate higher-resolution geochemical methods and multi-proxy datasets to refine the understanding of monsoon-ITCZ interactions in the tropical Indo-Pacific.

ACKNOWLEDGMENT

This study was supported by the Directorate General of Higher Education, Ministry of Education and Culture, Republic of Indonesia, through a research grant awarded to Aswan, Khoiril Anwar Maryunani, and Ryan Dwi Wahyu Ardi (contract no. 083/E5/PG.02.00.PT/2022). We sincerely thank the Research Center for Oceanography, LIPI, and especially Udhi Hermawan, chief scientist of the E-WIN 2016 expedition, for permitting the use of expedition data and for administrative assistance. Our appreciation is also extended to Singgih Prasetyo Adi Wibowo and the crew of the Baruna Jaya VIII research vessel for their technical support during data collection. Laboratory facilities and assistance provided by the Research Center for Geological Disaster, National Research and Innovation Agency, are also gratefully acknowledged.

REFERENCES

Andersen, K.K., Bigler, M., Buchardt, S.L., Clausen, H.B., Dahl-Jensen, D., Davies, S.M., Fischer, H., Goto-Azuma, K., Hansson, M.E., Heinemeier, J., Johnsen, S.J., Larsen, L.B., Muscheler, R. (2007). *Greenland Ice Core Chronology 2005 (GICC05) and 20 Year Means of Oxygen Isotope Data From Ice Core NGRIP*. AGU Fall Meeting Abstracts.

Ardi, R.D.W., Aswan, Maryunani, K.A., Yulianto, E., Putra, P.S., Nugroho, S.H., & Istiana. (2020). Last Deglaciation—Holocene Australian-Indonesian Monsoon Rainfall Changes Off Southwest Sumba, Indonesia. *Atmosphere,* 11(9), 932. https://doi.org/10.3390/atmos11090932.

Arz, H.W., Lamy, F., Ganopolski, A., Nowaczyk, N., & Pätzold, J. (2007). Dominant Northern Hemisphere Climate Control Over Millennial-Scale Glacial Sea-Level Variability. *Quaternary Science Reviews,* 26(3–4), 312–321. https://doi.org/10.1016/j.quascirev.2006.07.016.

Ayliffe, L.K., Gagan, M.K., Zhao, J., Drysdale, R. N., Hellstrom, J.C., Hantoro, W.S., Griffiths, M.L., Scott-gagan, H., Pierre, E. S., Cowley, J. A., & Suwargadi, B.W. (2013). Rapid Interhemispheric Climate Links Via The Australasian Monsoon During The Last Deglaciation. *Nature Communications*, 4 (May), 1–6. https://doi.org/10.1038/ncomms 3908.

Bayhaqi, A., Lenn, Y.D., Surinati, D., Polton, J., Nur, M., Corvianawatie, C., & Purwandana, A. (2019). The Variability of Indonesian Throughflow in Sumba Strait and Its Linkage to the Climate Events. *American Journal of Applied Sciences,* 16(4), 118–133. https://doi.org/10.3844/ajassp.2019.118.133.

Berger, A.L. (1978). Long-Term Variations of Daily Insolation and Quaternary Climatic Changes. *Journal of the Atmospheric Sciences,* 35(12), 2362–2367. https://doi.org/10.1175/1520-0469(1978)035<2362:LTVODI>2.0.CO;2

Bird, M.I., Taylor, D., & Hunt, C. (2005). Palaeoenvironments of Insular Southeast Asia During The Last Glacial Period: A Savanna Corridor in Sundaland? *Quaternary*

Science Reviews, 24(20–21), 2228–2242. https://doi.org/10.1016/j.quascirev.2005.04.004

Blaauw, M. (2010). Methods and Code For 'Classical' Age-Modelling of Radiocarbon Sequences. *Quaternary Geochronology,* 5(5), 512–518. https://doi.org/10.1016/j.quageo.2010.01.002>.

Blaauw, M. & Christen, J.A. (2011). Flexible Paleoclimate Age-Depth Models Using An Autoregressive Gamma Process. *Bayesian Analysis,* 6(3), 457–474. https://doi.org/10.1214/11-BA618

Broccoli, A.J., Dahl, K.A., & Stouffer, R.J. (2006). Response of the ITCZ to Northern Hemisphere Cooling. *Geophysical Research Letters,* 33(1). https://doi.org/10.1029/2005GL024546.

Chen, J., An, Z., & Head, J. (1999). Variation of Rb/Sr Ratios in The Loess-Paleosol Sequences of Central China During The Last 130,000 Years and Their Implications For Monsoon Paleoclimatology. *Quaternary Research,* 51(3), 215–219. https://doi.org/10.1006/qres.1999.2038

Chen, L., Shen, H., Jia, Y., Wu, J., Li, X., Wei, L., & Wang, P. (2008). Environmental Change Inferred From Rb and Sr of Lacustrine Sediments in Huangqihai Lake, Inner Mongolia*. Journal of Geographical Sciences,* 18(3), 373–384. https://doi.org/10.1007/s11442-008-0373-1.

Cui, T., Zhang, X., Li, Q., Wei, R., Li, X. & Wang, Y., (2025). Hydroclimate Variability in The Tropical Indo-Pacific During The Last Glacial Cycle. *Quaternary Science Reviews*, 330, p.108125. https://doi.org/10.1016/j.quascirev.2024.108125

Denniston, R.F., Ummenhofer, C.C., Wanamaker, A.D., Lachniet, M.S., Villarini, G., Asmerom, Y., Polyak, V.J., Passaro, K.J., Cugley, J., Woods, D., & Humphreys, W.F. (2016). Expansion and Contraction of The Indo-Pacific Tropical Rain Belt Over The Last Three Millennia. *Scientific Reports,* 6(1), 34485. https://doi.org/10.1038/srep34485

Di Nezio, P. N., Timmermann, A., Tierney, J. E., Jin, F., Otto-Bliesner, B., Rosenbloom, N., Mapes, B., Neale, R., Ivanovic, R. F., & Montenegro, A. (2016). The Climate Response of The Indo-Pacific Warm Pool to Glacial Sea Level. *Paleoceanography,* 31(6), 866–894. https://doi.org/10.1002/2015PA002890

EPICA Community Members (2006). One-to-One Coupling of Glacial Climate Variability in Greenland and Antarctica. *Nature,* 444(7116), 195–198. https://doi.org/10.1038/ nature05301

Feng, M., Meyers, G., Pearce, A., & Wijffels, S. (2003). Annual and Interannual Variations of The Leeuwin Current at 32°S. *Journal of Geophysical Research: Oceans,* 108(C11). https://doi.org/10.1029/2002JC001763

Feng, M., Zhang, N., Liu, Q., & Wijffels, S. (2018). The Indonesian Throughflow, Its Variability and Centennial Change. *Geoscience Letters*, 5(1). https://doi.org/10.1186/s40562-018-0102-2

Gebregiorgis, D., Giosan, L., Hathorne, E. C., Anand, P., Nilsson-Kerr, K., Plass, A., Lückge, A., Clemens, S. C., & Frank, M. (2020). What Can We Learn From X-Ray Fluorescence Core Scanning Data? A Paleomonsoon Case Study. *Geochemistry, Geophysics, Geosystems*, 21(2), 1–17. https://doi.org/10.1029/2019GC008414

Gordon, A. (2005). Oceanography of The Indonesian Seas and Their Throughflow. *Oceanography,* 18(4), 14–27. https://doi.org/10.5670/oceanog.2005.01

Griffiths, M. L., Drysdale, R. N., Gagan, M. K., Zhao, J. X., Ayliffe, L. K., Hellstrom, J. C., Hantoro, W. S., Frisia, S., Feng, Y. X., Cartwright, I., Pierre, E. S., Fischer, M. J., & Suwargadi, B. W. (2009). Increasing Australian-Indonesian Monsoon Rainfall Linked To Early Holocene Sea-Level Rise. *Nature Geoscience*, 2(9), 636–639. https://doi.org/10.1038/ngeo605

Hanebuth, T., Stattegger, K., & Grootes, P. M. (2000). Rapid Flooding of the Sunda Shelf: A Late-Glacial Sea-Level Record. *Science*, 288(5468), 1033–1035. https://doi.org/10.1126/science.288.5468.1033

Hendrizan, M., Kuhnt, W., & Holbourn, A. (2017). Variability of Indonesian Throughflow and Borneo Runoff During the Last 14 kyr. *Paleoceanography,* 32(10), 1054–1069. https://doi.org/10.1002/2016PA003030

Hendrizan, M., Kuhnt, W., Holbourn, A., Cahyarini, S. Y., & Ningsih, N. S. (2023). Kalimantan Hydroclimate Variability Since The Last Glacial Period. *International Journal of Earth Sciences,* 112(2), 615–629. https://doi.org/10.1007/s00531-022-02266-2

Holbourn, A., Kuhnt, W., Kawamura, H., Jian, Z., Grootes, P., Erlenkeuser, H., & Xu, J. (2005). Orbitally Paced Paleoproductivity Variations in The Timor Sea and Indonesian Throughflow Variability During The Last 460 kyr. *Paleoceanography*, 20(3), 1–18. https://doi.org/10.1029/2004PA001094

Kuhnt, W., Holbourn, A., Xu, J., Opdyke, B., De Deckker, P., Röhl, U., & Mudelsee, M. (2015). Southern Hemisphere Control on Australian Monsoon Variability During The Late Deglaciation and Holocene. *Nature Communications,* 6(1), 1–7. https://doi.org/10.1038/ncomms6916

Lim, S. Y., Marzin, C., Xavier, P., Chang, C. P., & Timbal, B. (2017). Impacts of Boreal Winter Monsoon Cold Surges and The Interaction With MJO on Southeast Asia Rainfall. *Journal of Climate,* 30(11), 4267–4281. https://doi.org/10.1175/JCLI-D-16-0546.1

Linsley, B. K., Rosenthal, Y., & Oppo, D. W. (2010). Holocene Evolution of The Indonesian Throughflow and The Western Pacific Warm Pool. *Nature Geoscience*, 3(8), 578–583. https://doi.org/10.1038/ngeo920

Lowry, D.P. & McGowan, H.A., 2024. Intensification of Monsoonal Precipitation in The Tropical Western Pacific During The Early Holocene. *Earth and Planetary Science Letters,* 617, p.118267. https://doi.org/10.1016/j.epsl.2023.118267

McGee, D., Donohoe, A., Marshall, J., & Ferreira, D. (2014). Changes in ITCZ Location and Cross-Equatorial Heat Transport at The Last Glacial Maximum, Heinrich Stadial 1, and The Mid-Holocene. *Earth and Planetary Science Letters,* 390, 69–79. https://doi.org/10.1016/j.epsl.2013.12.043

Miriyala, P., Sukumaran, N. P., Nath, B. N., Ramamurty, P. B., Sijinkumar, A. V., Vijayagopal, B., Ramaswamy, V., & Sebastian, T. (2017). Increased Chemical Weathering During The Deglacial To Mid-Holocene Summer Monsoon Intensification. *Scientific Reports,* 7(1), 44310. https://doi.org/10.1038/srep44310

Mohtadi, M., Oppo, D. W., Steinke, S., Stuut, J. B. W., De Pol-Holz, R., Hebbeln, D., & Lückge, A. (2011). Glacial to Holocene Swings of The Australian-Indonesian Monsoon. *Nature Geoscience,* 4(8), 540–544. https://doi.org/10.1038/ngeo1209

Mohtadi, M., Prange, M., Schefuß, E., & Jennerjahn, T. C. (2017). Late Holocene Slowdown of The Indian Ocean Walker Circulation. *Nature Communications*, 8(1). https://doi.org/10.1038/s41467-017-00855-3

Nesbitt, H. W., Markovics, G., & Price, R. C. (1980). Chemical Processes Affecting Alkalis and Alkaline Earths During Continental Weathering. *Geochimica et Cosmochimica Acta,* 44(11), 1659–1666. https://doi.org/10.1016/0016-7037(80)90218-5

Partin, J. W., Cobb, K. M., Adkins, J. F., Clark, B., & Fernandez, D. P. (2007). Millennial-scale Trends in West Pacific Warm Pool Hydrology Since The Last Glacial Maximum. *Nature*, 449(7161), 452–455. https://doi.org/10.1038/nature06164

Qu, T., Du, Y., Strachan, J., Meyers, G., & Slingo, J. (2005). Sea Surface Temperature and Its Variability in the Indonesian Region. *Oceanography,* 18(4), 50–61. https://doi.org/10.5670/oceanog.2005.05

R Core Team. (2013). A Language and Environment for Statistical Computing. In R Foundation for Statistical Computing (4.0.2). *R Foundation for Statistical Computing*. http://www.r-project.org

Scroxton, N., White, S.M., McGee, D. & Donnelly, J.P., 2022. ITCZ Shifts Drive Decoupled Monsoon Dynamics in The Tropical Indo-Pacific During The Last Deglaciation. *Science Advances,* 8(38), p.eabn0062. https://doi.org/10.1126/sciadv.abn0062

Setiawan, R. Y., Mohtadi, M., Southon, J., Groeneveld, J., Steinke, S., & Hebbeln, D. (2015). The Consequences of Opening The Sunda Strait on The Hydrography of The Eastern Tropical Indian Ocean. *Paleoceanography,* 30(10), 1358–1372. https://doi.org/10.1002/2015PA002802

Shackleton, N. J. (1987). Oxygen Isotopes, Ice Volume and Sea Level. *Quaternary Science Reviews,* 6(3–4), 183–190. https://doi.org/10.1016/0277-3791(87)90003-5

Siddall, M., Rohling, E. J., Almogi-Labin, A., Hemleben, Ch., Meischner, D., Schmelzer, I., & Smeed, D. A. (2003). Sea-level Fluctuations During The Last Glacial Cycle. *Nature,* 423(6942), 853–858. https://doi.org/10.1038/nature01690

Sprintall, J., & Révelard, A. (2014). The Indonesian Throughflow Response To Indo-Pacific Climate Variability. *Journal of Geophysical Research: Oceans,* 119(2), 1161–1175. https://doi.org/10.1002/2013JC009533

Sprintall, J., Wijffels, S. E., Molcard, R., & Jaya, I. (2009). Direct Estimates of The Indonesian Throughflow Entering The Indian Ocean: 2004-2006. *Journal of Geophysical Research: Oceans,* 114(7), 2004–2006. https://doi.org/10.1029/2008JC005257

Stott, L., Timmermann, A., & Thunell, R. (2007). Southern Hemisphere and Deep-Sea Warming Led Deglacial Atmospheric CO 2

Rise and Tropical Warming. *Science,* 318(5849), 435–438. https://doi.org/10.1126/science.1143791

Suppiah, R., & Wu, X. (1998). Surges, Cross-Equatorial Flows and Their Links With The Australian Summer Monsoon Circulation And Rainfall. *Australian Meteorological Magazine*, 47(2), 113–130.

Tjallingii, R., Röhl, U., Kölling, M., & Bickert, T. (2007). Influence of The Water Content on X-Ray Fluorescence Corescanning Measurements in Soft Marine Sediments. *Geochemistry, Geophysics, Geosystems,* 8(2). https://doi.org/10.1029/2006GC001393

Wang, P. X., Wang, B., Cheng, H., Fasullo, J., Guo, Z., Kiefer, T., & Liu, Z. (2017). The Global Monsoon Across Time Scales: Mechanisms and Outstanding Issues. *Earth-Science Reviews,* 174(July 2016), 84–121. https://doi.org/10.1016/j.earscirev.2017.07.006

Wang, Y., Cheng, H., Edwards, R. L., He, Y., Kong, X., An, Z., Wu, J., Kelly, M. J., Dykoski, C. A., & Li, X. (2005). The Holocene Asian Monsoon: Links to Solar Changes and North Atlantic Climate. *Science,* 308(5723), 854–857. https://doi.org/10.1126/science.1106296

Xu, J., Kuhnt, W., Holbourn, A., Regenberg, M., & Andersen, N. (2010). Indo-pacific Warm Pool Variability During The Holocene and Last Glacial Maximum. *Paleoceanography*, 25(4). https://doi.org/10.1029/2010PA001934

Yu, J., Kuhnt, W., Lückge, A., Scheeder, G. & Westphal, H., 2023. Orbital- and Millennial-Scale Rainfall Variability in The Tropical Indo-Pacific During The Last 150,000 Years. *Quaternary Science Reviews,* 311, p.107834. https://doi.org/10.1016/j.quascirev.2023.107834